

**<sup>18</sup>F-AIF-NOTA-octreotide outperforms <sup>68</sup>Ga-DOTA-TATE/-NOC PET in neuroendocrine tumor patients: results from a prospective, multicenter study**

Elin Pauwels<sup>1</sup>, Frederik Cleeren<sup>2</sup>, T rence Tshibangu<sup>2</sup>, Michel Koole<sup>1</sup>, Kim Serdons<sup>1</sup>, Lennert Boeckxstaens<sup>1</sup>, Jeroen Dekervel<sup>3</sup>, Timon Vandamme<sup>4,5</sup>, Willem Lybaert<sup>5</sup>, Bliede Van den Broeck<sup>6</sup>, Annouschka Laenen<sup>7</sup>, Paul M. Clement<sup>8</sup>, Karen Geboes<sup>9</sup>, Eric Van Cutsem<sup>3</sup>, Sigrid Stroobants<sup>10</sup>, Chris Verslype<sup>3</sup>, Guy Bormans<sup>2</sup>, Christophe M. Deroose<sup>1</sup>

<sup>1</sup>Nuclear Medicine, University Hospitals Leuven & Nuclear Medicine and Molecular Imaging, Department of Imaging and Pathology, KU Leuven, Leuven, Belgium;

<sup>2</sup>Radiopharmaceutical Research, Department of Pharmacy and Pharmacology, KU Leuven, Leuven, Belgium;

<sup>3</sup>Digestive Oncology, University Hospitals Leuven, Leuven, Belgium;

<sup>4</sup>Center for Oncological Research (CORE), Integrated Personalized and Precision Oncology Network (IPPON), University of Antwerp, Antwerp, Belgium;

<sup>5</sup>Oncology, NETwerk Antwerpen-Waasland CoE, Belgium;

<sup>6</sup>Nuclear Medicine, Ghent University Hospital, Ghent, Belgium;

<sup>7</sup>Leuven Biostatistics and Statistical Bioinformatics Center, KU Leuven, Leuven, Belgium;

<sup>8</sup>General Medical Oncology, University Hospitals Leuven, Leuven, Belgium;

<sup>9</sup>Digestive Oncology, Department of Gastroenterology, Ghent University Hospital, Ghent, Belgium;

<sup>10</sup>Nuclear Medicine, Antwerp University Hospital & Molecular Imaging and radiology, Faculty of Medicine and Health Sciences, University of Antwerp, Wilrijk, Belgium

**Corresponding author:** Christophe M. Deroose

Address: UZ Leuven, Nucleaire Geneeskunde, Herestraat 49, BE-3000 Leuven, Belgium

Telephone: +3216343715; Fax: +3216343759; [christophe.deroose@uzleuven.be](mailto:christophe.deroose@uzleuven.be)

ORCID-ID: 0000-0002-6080-1577

**First author:** Elin Pauwels MD, PhD student

Address: UZ Leuven, Nucleaire Geneeskunde, Herestraat 49, BE-3000 Leuven, Belgium

Telephone: +3216343715; [elin.pauwels@uzleuven.be](mailto:elin.pauwels@uzleuven.be)

ORCID-ID: 0000-0002-3296-8011

**Word count:** 5000

**ClinicalTrials.gov:** NCT04552847

**Financial support:** This research was funded by the project from "Kom op tegen Kanker": "PET/MR imaging of the norepinephrine transporter and somatostatin receptor in neural crest and neuroendocrine tumors for better radionuclide therapy selection".

CMD is a Senior Clinical Investigators at Research Foundation-Flanders (FWO).

**Running title:** <sup>18</sup>F-AIF-OC vs. <sup>68</sup>Ga-DOTA-SSA PET

## ABSTRACT

Fluorine-18-labeled somatostatin analogs (SSAs) could represent a valid alternative to the current gold standard gallium-68-labeled SSAs for somatostatin receptor (SSTR) imaging in patients with neuroendocrine tumors (NETs), given their logistical advantages. Recently,  $^{18}\text{F}$ -AIF-NOTA-octreotide ( $^{18}\text{F}$ -AIF-OC) has emerged as a promising candidate, but a thorough comparison with  $^{68}\text{Ga}$ -DOTA-SSA in large patient groups is needed. This prospective, multicenter trial aims to demonstrate non-inferiority of  $^{18}\text{F}$ -AIF-OC compared with  $^{68}\text{Ga}$ -DOTA-SSA PET in NET patients (ClinicalTrials.gov: NCT04552847).

**Methods:** Seventy-five patients with histologically confirmed NET and a routine clinical  $^{68}\text{Ga}$ -DOTATATE (n=56) or  $^{68}\text{Ga}$ -DOTANOC (n=19) PET, performed within a 3-month interval of the study scan (median: 7 days; range: -30 to +32 days), were included. Patients underwent a whole-body PET, two hours after IV injection of 4 MBq/kg  $^{18}\text{F}$ -AIF-OC. A randomized, blinded consensus read was performed by two experienced readers to count tumor lesions. Following unblinding, the detection ratio (DR) was determined for each scan, i.e. the fraction of lesions detected on a scan compared to the union of lesions of both scans. The differential detection ratio (DDR; difference in DR between  $^{18}\text{F}$ -AIF-OC and  $^{68}\text{Ga}$ -DOTATATE/NOC) per patient was calculated. Tracer uptake was evaluated by comparing  $\text{SUV}_{\text{max}}$  and tumor-to-background ratios (TBRs) in concordant lesions.

**Results:** In total, 4709 different tumor lesions were detected, 3454 with  $^{68}\text{Ga}$ -DOTATATE/NOC and 4278 with  $^{18}\text{F}$ -AIF-OC. The mean DR with  $^{18}\text{F}$ -AIF-OC was significantly higher than with  $^{68}\text{Ga}$ -DOTATATE/NOC (91.1% vs. 75.3%;  $P < 10^{-5}$ ). The resulting mean DDR was 15.8% with a lower margin of the 95% confidence interval (95% CI: 9.6%–22.0%) higher than -15%, the pre-specified boundary for non-inferiority. The mean DDR for the  $^{68}\text{Ga}$ -DOTATATE and  $^{68}\text{Ga}$ -DOTANOC subgroups were 11.8% (95% CI: 4.3–19.3) and 27.5% (95% CI: 17.8–37.1), respectively. The mean DDR for most organs was higher than zero, except for bone lesions (mean DDR -2.8% (95%

CI: -17.8–12.2)). No significant differences in mean  $SUV_{max}$  were observed ( $P = 0.067$ ), but mean TBR was significantly higher with  $^{18}F$ -AIF-OC than with  $^{68}Ga$ -DOTATATE/NOC ( $31.7 \pm 36.5$  vs.  $25.1 \pm 32.7$ ;  $P=0.001$ ).

**Conclusion:**  $^{18}F$ -AIF-OC is non-inferior and even superior compared with  $^{68}Ga$ -DOTATATE/NOC PET in NET patients. This validates  $^{18}F$ -AIF-OC as an option for clinical practice SSTR PET.

**Keywords:**  $^{18}F$ -AIF-NOTA-octreotide;  $^{68}Ga$ -DOTATATE;  $^{68}Ga$ -DOTANOC; neuroendocrine tumor; somatostatin receptor

## INTRODUCTION

Neuroendocrine tumors (NETs) are part of a heterogeneous group of relatively rare tumors that develop from cells of the diffuse neuroendocrine system and are mainly found in the gastrointestinal and respiratory tract. Many NETs show an overexpression of the somatostatin receptor (SSTR), a G-protein coupled membrane receptor, that makes an excellent target for molecular imaging and therapy with radiolabeled somatostatin analogs (SSAs) (1). SSTR imaging plays a crucial role in the diagnostic work-up, treatment selection, follow-up and recurrence detection of NETs (1).  $^{68}\text{Ga}$ -1,4,7,10-tetraazacyclododecane-1,4,7,10-tetraacetic acid (DOTA)-Tyr<sup>3</sup>-octreotate ( $^{68}\text{Ga}$ -DOTATATE),  $^{68}\text{Ga}$ -DOTA-Tyr<sup>3</sup>-octreotide ( $^{68}\text{Ga}$ -DOTATOC) and  $^{68}\text{Ga}$ -DOTA-1-Nal<sup>3</sup>-octreotide ( $^{68}\text{Ga}$ -DOTANOC), which can be collectively referred to as  $^{68}\text{Ga}$ -DOTA-SSAs, are considered as the current gold standard for SSTR imaging (1,2). However, their widespread clinical implementation faces challenges inherent to the use of  $^{68}\text{Ge}/^{68}\text{Ga}$ -generators, such as limited availability, high associated costs and low activity yield per elution (3). These challenges can be largely overcome by a fluorine-18-labeled alternative. In particular, the high activity yield in combination with a favorable half-life of 109.8 minutes enables centralized production of fluorine-18-labeled tracers followed by distribution to distant positron emission tomography (PET) centers without cyclotron access (3). Furthermore, fluorine-18 has a shorter positron range than gallium-68 and is therefore more suitable for high spatial resolution imaging on modern PET cameras (3).

Recently,  $^{18}\text{F}$ -Al-1,4,7-triazacyclononane-1,4,7-tri-acetate-octreotide ( $^{18}\text{F}$ -AIF-NOTA-octreotide;  $^{18}\text{F}$ -AIF-OC) has emerged as a promising fluorine-18-labeled SSA for SSTR imaging (4,5).  $^{18}\text{F}$ -AIF-OC is synthesized using the chelator-based Al<sup>18</sup>F-method (6). To allow clinical implementation, a fast and robust automated good manufacturing practice-compliant process was recently developed (7). Two independently performed first clinical translations of  $^{18}\text{F}$ -AIF-OC in healthy volunteers and NET patients have reported favorable dosimetry, biodistribution, tracer

kinetics and lesion targeting (4,5). First comparisons of  $^{18}\text{F}$ -AIF-OC with  $^{68}\text{Ga}$ -DOTATATE in two small NET patient groups ( $n = 6$  and  $n = 20$ ) have shown similar lesion detection rates and tumor uptake (5,8). However, a thorough head-to-head comparison with  $^{68}\text{Ga}$ -DOTA-SSA PET in large patient groups is still lacking.

This prospective multicenter trial aimed to demonstrate that the diagnostic performance of  $^{18}\text{F}$ -AIF-OC PET is equivalent or superior to the current gold standard,  $^{68}\text{Ga}$ -DOTA-SSA PET, in NET patients (non-inferiority trial).

## **MATERIALS AND METHODS**

A full version of the Materials and Methods section is provided in the supplemental information.

### **Study Population**

In the main part (part A) of this prospective multicenter trial 75 NET patients, aged 18 years or older, were included. The main inclusion criteria were: (1) histologically and/or cytologically confirmed NET of all grades of gastroenteropancreatic, pulmonary, neural crest or unknown primary origin, (2) routine clinical  $^{68}\text{Ga}$ -DOTA-SSA PET/computed tomography (CT) scheduled within three months prior or after the study scan, (3) at least one known tumor lesion below the level of the submandibular and parotid glands, with either a minimum size of 1 cm in at least one dimension on morphological imaging (CT, magnetic resonance imaging (MRI) or ultrasound), or a maximal standardized uptake value ( $\text{SUV}_{\text{max}}$ ) of at least 10 on  $^{68}\text{Ga}$ -DOTA-SSA PET. The main exclusion criterion was previous or ongoing recurrent or chronic disease at high risk to interfere with the performance or evaluation of the trial. The PET/MR part (part B) of the trial in 10 NET patients will be presented elsewhere.

The study was performed at University Hospitals Leuven in collaboration with University Hospital Antwerp and University Hospital Ghent after approval by the Ethics Committee of all three institutes, and all subjects signed a written informed consent (ClinicalTrials.gov identifier: NCT04552847, EudraCT: 2020-000549-15).

### **PET/CT Acquisition**

We previously identified 2 hours post-injection (p.i.) to be the optimal time point for imaging (5). Patients underwent a whole-body PET (from mid-thigh to vertex) 2 hours after intravenous (IV) injection of 4 MBq/kg  $^{18}\text{F}$ -AIF-OC, preceded by a low-dose CT for attenuation correction and anatomical information.

For both the routine and study scan, patients were asked to avoid long-acting SSA treatment, except in case of uncontrolled hormonal symptoms, for four to six weeks prior to the scan.

### **Image Analyses**

All image analyses were done using MIM v7.1.5. Tumor lesions were counted in consensus by two experienced readers, blinded for patient data and the radiopharmaceutical that was used. Routine and study scans were randomized per group of 20 patients (40 scans per group) and information regarding patient and radiopharmaceutical was removed from the DICOM headers. Furthermore, since normal salivary gland uptake is markedly higher with  $^{68}\text{Ga}$ -DOTATATE compared with  $^{18}\text{F}$ -AIF-OC (5,8), all PET datasets were trimmed by an independent operator to remove the head region. A positive lesion was defined as a volume of increased tracer uptake compared to background, deemed to be caused by the presence of NET cells, and that is unlikely to be attributed to physiological or benign etiology (e.g. inflammation, blood pool retention, excretion, etc.). A detailed description of the consensus read is provided in the supplemental information.

Following unblinding, the detection ratio (DR) was determined for each scan, i.e. the fraction of lesions detected on that scan, using the union of lesions detected by both tracers ( $^{68}\text{Ga}$ -DOTATATE/NOC and  $^{18}\text{F}$ -AIF-OC) in a patient as the reference. Finally, the differential detection ratio (DDR), which is the difference in DR between  $^{18}\text{F}$ -AIF-OC and  $^{68}\text{Ga}$ -DOTATATE/NOC, was calculated for each patient. The DR at organ level was determined as the number of lesions detected with one tracer divided by all lesions detected by both tracers in a specific organ.

For each lesion, the  $\text{SUV}_{\text{max}}$  was measured and the tumor-to-background ratio (TBR) was calculated by dividing the  $\text{SUV}_{\text{max}}$  of that lesion by the  $\text{SUV}_{\text{mean}}$  of relevant background tissue (liver for liver lesions, bone for bone lesions and gluteal muscle for all other lesions). In patients for whom no healthy liver ( $n=1$ ) or bone tissue ( $n=2$ ) could be delineated, the mean background value of all other patients was used instead to determine TBRs. Lesions with incorrect attenuation correction due to PET-CT misregistration were excluded from semi-quantitative analysis.

## Outcomes

The primary outcome measure was the DDR. The primary objective, i.e. non-inferiority of  $^{18}\text{F}$ -AIF-OC compared with  $^{68}\text{Ga}$ -DOTATATE/NOC, would be met if the lower margin of the 95% confidence interval (95% CI) for the mean DDR was higher than -15%.

Secondary outcome measures included: lesion uptake in matched pairs of lesions ( $\text{SUV}_{\text{max}}$  and TBR); DR and DDR at organ level; DDR in function of the specific  $^{68}\text{Ga}$ -DOTA-SSA used ( $^{68}\text{Ga}$ -DOTATATE or  $^{68}\text{Ga}$ -DOTANOC) and tumor grade; impact of  $^{18}\text{F}$ -AIF-OC administration on blood pressure and heart rate. A posthoc analysis according to primary tumor site (for  $n>10$ ) was performed as well.

Lesion uptake was assessed (a) at patient level, (b) for two subsets of hottest lesions, i.e. 20 lesions per patient and maximum 5 lesions per organ, at patient level and (c) at lesion level. Note that for secondary outcome measures, tumor lesions in the head region, identified through non-

blinded consensus read, were added in the analyses. The safety evaluation is provided in the supplemental information.

## RESULTS

### Patients and $^{18}\text{F}$ -AIF-OC Administration

Patient and clinical characteristics are shown in Table 1. The median time between  $^{18}\text{F}$ -AIF-OC and routine  $^{68}\text{Ga}$ -DOTATATE/NOC scan was 7 days (range -30–32), with 52 patients (78.7%) having both scans within a 15-day interval (Supplemental Figure 1). No therapeutic changes occurred between the scans, except in three patients: in two patients, everolimus was added 2 days and 7 days before the second scan ( $^{18}\text{F}$ -AIF-OC), respectively, and in one patient, SSA treatment was reinitiated 13 days before the second scan ( $^{18}\text{F}$ -AIF-OC). The mean injected activity and peptide mass of  $^{18}\text{F}$ -AIF-OC were  $295\pm 60$  MBq and  $11.2\pm 6.8$   $\mu\text{g}$ , respectively.

### Detection Rate Analysis

During blinded consensus read, 4709 different tumor lesions were counted, 3454 with  $^{68}\text{Ga}$ -DOTATATE/NOC and 4278 with  $^{18}\text{F}$ -AIF-OC. In 48 patients,  $^{18}\text{F}$ -AIF-OC detected more lesions than  $^{68}\text{Ga}$ -DOTATATE/NOC, whereas  $^{68}\text{Ga}$ -DOTATATE/NOC detected more lesions in only 15 patients. The mean DR with  $^{18}\text{F}$ -AIF-OC was significantly higher than with  $^{68}\text{Ga}$ -DOTATATE/NOC (91.1% vs. 75.3%;  $P < 10^{-5}$ ). The resulting mean DDR was 15.8% (95% CI: 9.6%–22.0%). As the lower margin of the 95% CI was higher than -15%, the primary objective of the trial was met. DDR values ranged from -74.2% to 77.5% (interquartile range: 0.0%–32.7%) (Supplemental Figure 2).

In the head region, 214 additional lesions were counted. A summary of results for the most relevant organs is provided in Table 2. A full analysis at organ level is shown in Supplemental Table 1. Organs where most lesions were observed were bone (2012 lesions in 50 patients),

followed by liver (1739 lesions in 54 patients), lymph nodes (602 lesions in 63 patients), peritoneum (275 lesions in 28 patients) and lung (195 lesions in 18 patients). The mean DR for these sites were significantly higher with  $^{18}\text{F}$ -AIF-OC compared with  $^{68}\text{Ga}$ -DOTATATE/NOC with mean DDR values well above zero, except for bone, where the DR with both tracers was similar (79.8% vs. 77.0%; mean DDR -2.8% (95% CI: -17.8–12.2)).

Both within the  $^{68}\text{Ga}$ -DOTATATE and the  $^{68}\text{Ga}$ -DOTANOC subgroups, the mean DR with  $^{18}\text{F}$ -AIF-OC was significantly higher than with  $^{68}\text{Ga}$ -DOTATATE or -NOC (Table 3). The mean DDR for the  $^{68}\text{Ga}$ -DOTATATE subgroup was 11.8% (95% CI: 4.3–19.3) versus 27.5% (95% CI: 17.8–37.1) for the  $^{68}\text{Ga}$ -DOTANOC subgroup. The detailed analysis is shown in Supplemental Table 2 and 3.

Subgroup analysis according to tumor grade showed a similar mean DDR for G1 and G2 tumors (14.9% (95% CI: 6.0–23.8) vs. 16.6 (95% CI: 6.3–27.0), respectively) (Table 3). The mean DDR for the G3 subgroup was 35.4%. However, as this group contained only two patients, no statistics could be applied. No significant correlation was observed between Ki-67 index and DDR (Spearman correlation coefficient ( $\rho$ )=0.075,  $P$ =0.54; Supplemental Figure 3).

Finally, the mean DR for patients with a NET from intestinal origin was significantly higher with  $^{18}\text{F}$ -AIF-OC than with  $^{68}\text{Ga}$ -DOTATATE/NOC (mean DDR 17.8% (95% CI: 9.2–26.4)), whereas no significant differences were observed for patients with a pancreatic NET (Table 3).

The forest plot in Figure 1 summarizes the results of the DR analysis. Head-to-head comparisons with examples of missed lesions are shown in Figure 2 and 3.

## **Lesion Uptake**

Mean  $\text{SUV}_{\text{max}}$  at patient level showed a trend toward lower values with  $^{18}\text{F}$ -AIF-OC compared with  $^{68}\text{Ga}$ -DOTATATE/NOC, but this was not statistically significant (20.0 vs. 22.4;  $P$ =0.067). On the other hand, TBR was significantly higher with  $^{18}\text{F}$ -AIF-OC (31.7 vs. 25.1;  $P$ =0.001) (Table 4; Figure 4). Of note, background uptake was significantly lower with  $^{18}\text{F}$ -AIF-OC

compared with  $^{68}\text{Ga}$ -DOTATATE/NOC ( $4.2\pm 1.7$  vs.  $6.3\pm 2.5$  ( $P<10^{-7}$ ),  $0.7\pm 0.2$  vs.  $1.2\pm 0.5$  ( $P<10^{-7}$ ) and  $0.4\pm 0.1$  vs.  $0.6\pm 0.2$  ( $P<10^{-7}$ ) for healthy liver, bone and muscle, respectively; Supplemental Table 4). At lesion level,  $\text{SUV}_{\text{max}}$  was significantly lower and TBR significantly higher with  $^{18}\text{F}$ -AIF-OC compared with  $^{68}\text{Ga}$ -DOTATATE/NOC (mean difference:  $-2.21$  (95% CI:  $-4.28 - -0.15$ ),  $P=0.036$  and  $8.47$  (95% CI:  $3.46-13.49$ ),  $P=0.001$  for  $\text{SUV}_{\text{max}}$  and TBR, respectively). Similar results were observed for a subset of maximum 20 hottest lesions per patient and 5 hottest lesions per organ (Table 4). Of note, considerable variation in lesion uptake was also observed within the same patient, with higher  $\text{SUV}_{\text{max}}$  with  $^{18}\text{F}$ -AIF-OC in some lesions and higher  $\text{SUV}_{\text{max}}$  with  $^{68}\text{Ga}$ -DOTATATE/NOC in others. Lesion uptake (at patient level) per organ is shown in Table 4 and Supplemental Table 5. For the three most common metastatic sites (liver, bone and lymph nodes), TBR was significantly higher with  $^{18}\text{F}$ -AIF-OC compared with  $^{68}\text{Ga}$ -DOTATATE/NOC. However, only bone lesions showed a significantly lower  $\text{SUV}_{\text{max}}$  with  $^{18}\text{F}$ -AIF-OC. Lesion uptake at patient level for patient subgroups according to routine  $^{68}\text{Ga}$ -DOTA-SSA tracer, tumor grade and primary is summarized in Table 5 (Supplemental Table 6: per organ analysis). Most strikingly, mean  $\text{SUV}_{\text{max}}$  with  $^{68}\text{Ga}$ -DOTANOC was significantly lower than with  $^{18}\text{F}$ -AIF-OC, overall and in particular also for liver, lymph node and peritoneal lesions. Other subgroup results were in line with results for the whole patient group.

The Bland-Altman plot showed a fair agreement between mean  $\text{SUV}_{\text{max}}$  with  $^{18}\text{F}$ -AIF-OC and  $^{68}\text{Ga}$ -DOTATATE/NOC, with a bias toward higher  $\text{SUV}_{\text{max}}$  in the  $^{68}\text{Ga}$ -DOTATATE subgroup and lower  $\text{SUV}_{\text{max}}$  in the  $^{68}\text{Ga}$ -DOTANOC subgroup compared with  $^{18}\text{F}$ -AIF-OC (Supplemental Figure 4).

## DISCUSSION

This prospective trial aimed to demonstrate non-inferiority of  $^{18}\text{F}$ -AIF-OC compared with  $^{68}\text{Ga}$ -DOTA-SSA PET in NET patients. The objective would be met if the lower margin of the 95%

CI for the mean DDR was higher than -15%. We observed a mean DDR of 15.8% (95% CI: 9.6%–22.0%), demonstrating superiority of  $^{18}\text{F}$ -AIF-OC compared with  $^{68}\text{Ga}$ -DOTATATE/NOC. Per organ analysis showed that  $^{18}\text{F}$ -AIF-OC outperforms  $^{68}\text{Ga}$ -DOTATATE/NOC with DRs around 90% or higher for most sites, with bone being the most important exception. Overall, lesions missed by  $^{18}\text{F}$ -AIF-OC were mainly situated in bone, in line with our previous findings (5). Nevertheless, the diagnostic performance for bone lesions of  $^{18}\text{F}$ -AIF-OC was similar to that of  $^{68}\text{Ga}$ -DOTATATE/NOC (DR around 80%; mean DDR -2.8%). Results for the  $^{68}\text{Ga}$ -DOTATATE and  $^{68}\text{Ga}$ -DOTANOC subgroups were more or less in line with the results for the total patient group, except for bone lesions for which  $^{68}\text{Ga}$ -DOTATATE showed a significantly higher DR compared with  $^{18}\text{F}$ -AIF-OC, while  $^{68}\text{Ga}$ -DOTANOC had a significantly lower DR. The DDR was higher in the  $^{68}\text{Ga}$ -DOTANOC subgroup than in the  $^{68}\text{Ga}$ -DOTATATE subgroup, implying that  $^{18}\text{F}$ -AIF-OC outperforms  $^{68}\text{Ga}$ -DOTANOC even more than  $^{68}\text{Ga}$ -DOTATATE. The G1 and G2 subgroup had a similar DDR (insufficient data for G3 tumors) and no associations between Ki-67 index and DDR were observed. The DR analysis for patients with a NET from intestinal origin was similar to the whole patient cohort, whereas for patients with a pancreatic NET,  $^{18}\text{F}$ -AIF-OC and  $^{68}\text{Ga}$ -DOTATATE/NOC performed equally well.

Lesion uptake in terms of TBR, which is the most important parameter for lesion detectability, was significantly higher for  $^{18}\text{F}$ -AIF-OC compared with  $^{68}\text{Ga}$ -DOTATATE/NOC, both at patient level and lesion level, as well as for most organs, including bone. This is reflected in the overall higher DRs for  $^{18}\text{F}$ -AIF-OC. On the other hand in comparison with  $\text{SUV}_{\text{max}}$  with  $^{68}\text{Ga}$ -DOTATATE/NOC,  $\text{SUV}_{\text{max}}$  with  $^{18}\text{F}$ -AIF-OC was either significantly lower, e.g. at lesion level, for subsets of hottest lesions per patient and for bone lesions, or similar, e.g. at patient level and for most organs. These results are in line with our previous findings (5), but slightly differ from those of Hou et al. (8) since they not only observed higher TBRs, but also higher  $\text{SUV}_{\text{max}}$  with  $^{18}\text{F}$ -AIF-OC compared with  $^{68}\text{Ga}$ -DOTATATE, although the latter was not statistically significant. Nevertheless, higher TBR values for  $^{18}\text{F}$ -AIF-OC are mainly explained by significantly lower

background uptake. In particular, the lower background uptake with  $^{18}\text{F}$ -AIF-OC in the liver significantly improves detection of liver metastases as reflected by the high DDR value of 33.1% (95% CI: 21.7%–44.4%), which is consistent with previous observations (5,8). Tracer clearance may partly explain the lower background values for  $^{18}\text{F}$ -AIF-OC, as  $^{18}\text{F}$ -AIF-OC imaging was done at a later time point (2h p.i.) than  $^{68}\text{Ga}$ -DOTATATE (45–60 min. p.i.) or  $^{68}\text{Ga}$ -DOTANOC (45–60 min. p.i.) imaging. However, Hou et al. (8) also reported a 1.5 times lower liver background with  $^{18}\text{F}$ -AIF-OC at 60 min. p.i., compared with  $^{68}\text{Ga}$ -DOTATATE (50 min. p.i.), as well as significantly lower bone background.

Lesion uptake for the  $^{68}\text{Ga}$ -DOTATATE subgroup was similar to the whole patient cohort. On the other hand, in the  $^{68}\text{Ga}$ -DOTANOC subgroup mean  $\text{SUV}_{\text{max}}$  values were significantly lower with  $^{68}\text{Ga}$ -DOTANOC compared with  $^{18}\text{F}$ -AIF-OC, in line with findings from a head-to-head comparison between  $^{68}\text{Ga}$ -DOTANOC and  $^{68}\text{Ga}$ -DOTATATE where significantly lower lesion  $\text{SUV}_{\text{max}}$  values were reported with  $^{68}\text{Ga}$ -DOTANOC (9). This can most likely be explained by differences in SSTR affinity profile, as  $^{68}\text{Ga}$ -DOTATATE has an almost ten-fold higher affinity for SSTR2 – the SSTR subtype that is most frequently expressed in NETs – than  $^{68}\text{Ga}$ -DOTANOC (9-11).

In accordance with Hou et al. (8), we observed considerable variability in lesion uptake both between and within patients. Differences in SSTR affinity profile between  $^{18}\text{F}$ -AIF-OC and  $^{68}\text{Ga}$ -DOTATATE/NOC – to our knowledge, the exact affinity profile for  $^{18}\text{F}$ -AIF-OC is still unknown – in combination with NET heterogeneity may lie at the basis of this finding. Of note, this variability has also been reported in a head-to-head comparison between  $^{68}\text{Ga}$ -DOTATATE and  $^{68}\text{Ga}$ -DOTATOC (12). In particular, the Bland-Altman plot of mean differences of mean  $\text{SUV}_{\text{max}}$  with  $^{68}\text{Ga}$ -DOTATATE and  $^{68}\text{Ga}$ -DOTATOC showed a similar range between the limits of agreement as we observed for mean  $\text{SUV}_{\text{max}}$  with  $^{18}\text{F}$ -AIF-OC and  $^{68}\text{Ga}$ -DOTATATE (12). As  $^{68}\text{Ga}$ -DOTATATE and  $^{68}\text{Ga}$ -DOTATOC are considered to be equivalent in clinical practice, we believe that the uptake variability for  $^{18}\text{F}$ -AIF-OC will also be of limited relevance for implementation in

routine practice. Furthermore, especially in case of disseminated disease, it is likely that  $^{18}\text{F}$ -AIF-OC and  $^{68}\text{Ga}$ -DOTATATE/NOC could be used interchangeably without clinical impact. A population that might benefit from  $^{18}\text{F}$ -AIF-OC are patients with confined liver disease in whom liver-directed therapies are considered.

The most important limitation of this trial is the lack of histological confirmation of all detected lesions due to ethical and practical reasons. Therefore, we did not have a perfect reference for evaluation of diagnostic performance as some lesions may have been false-positive. However, false-positive lesions are considered to be rare as in most cases additional lesions with one tracer compared to the other were observed in organs already known to be metastatically involved. Furthermore, in some cases, additional lesions observed with  $^{18}\text{F}$ -AIF-OC in previously unknown disease sites were later confirmed on  $^{68}\text{Ga}$ -DOTATATE/NOC follow-up imaging (Supplemental Figure 5). Secondly, due to practical reasons, it was not possible to organize the study scan within a day of the routine scan. Although kept to a minimum, in about 20% of patients the interval between both scans was more than 15 days (up to 32). However, as most patients had stable disease, especially those with a longer time between scans, the influence of the scan interval on results of the trial is deemed negligible. Thirdly, the time between long-acting SSA intake and scan was not standardized. However, a recent prospective study reported no significant changes in tumor uptake depending on the time since last SSA intake (13). Fourthly, in three patients a therapeutic change occurred between the two scans. Since the same number or more lesions were observed on the second scan, this will have no significant impact on the results of the study.

Finally, it is important to note the differences in imaging parameters, e.g. the higher administered activity and longer time between tracer administration and imaging with  $^{18}\text{F}$ -AIF-OC compared with  $^{68}\text{Ga}$ -DOTATATE/NOC, as these most likely have benefited the diagnostic performance of  $^{18}\text{F}$ -AIF-OC. However, these are examples of advantages of fluorine-18-labeled tracers over gallium-68-labeled tracers that should be exploited as the ultimate aim is to provide

an alternative tracer for clinical practice with beneficial manufacturing properties and increased cost-effectiveness compared with the current gold standard. Of note, the effective dose per injected activity is similar for  $^{18}\text{F}$ -AIF-OC and  $^{68}\text{Ga}$ -DOTA-SSAs (22.4  $\mu\text{Sv}/\text{MBq}$  vs. 21  $\mu\text{Sv}/\text{MBq}$ , respectively) (3,5). Future trials may focus on identifying the optimal activity in combination with PET acquisition time for  $^{18}\text{F}$ -AIF-OC.

## **CONCLUSION**

$^{18}\text{F}$ -AIF-OC demonstrated an excellent diagnostic performance, meeting our pre-specified criterion for non-inferiority and, even showing superiority compared with  $^{68}\text{Ga}$ -DOTATATE/NOC in NET patients. This validates  $^{18}\text{F}$ -AIF-OC as an option for clinical practice SSTR PET.

## **DISCLOSURE**

No conflicts of interest (Cols) relevant to this work exist. Non-related potential Cols include: TV has been a scientific advisor to Omnigen and a consultant for Sirtex, Ipsen and Novartis. PMC has received consulting fees and non-financial support from BMS and Bayer; consulting fees from Merck, Takeda, Rakuten and Leo; non-financial support from Teva and Novartis; and grants and non-financial support from AstraZeneca. KG has received consultancy fees and travel grants from MSD, BMS, Pierre Fabre and Servier. EVC has received advisory board fees from Array BioPharma, Astellas Pharma, AstraZeneca, Bayer, Bristol-Myers Squibb, Celgene, Daiichi Sankyo, Lilly, Roche, GlaxoSmithKline, Halozyme, Incyte, Ipsen, Merck, Novartis, Pierre Fabre, Sirtex and Taiho. CV has received research grants and performed consultancy services for Novartis, Ipsen and Bayer, outside the submitted work. CMD has been a consultant for Terumo, Ipsen, Sirtex, Bayer and PSI CRO.

## **ACKNOWLEDGMENTS**

The authors thank Prof. Kristof Baete, Mr. Wies Deckers and Mr. Stijn De Schepper of the medical physics team of UZ Leuven and UZ Antwerp, Mr. Kwinten Porters and Mr. Jef Van Loock, and the PET radiopharmacy team of UZ Leuven for their skilled contributions.

## **KEY POINTS**

**QUESTION:** Is the diagnostic performance of  $^{18}\text{F}$ -AIF-OC PET equivalent or superior to the current gold standard,  $^{68}\text{Ga}$ -DOTA-SSA PET, in NET patients?

**PERTINENT FINDINGS:** In this prospective, multicenter study in 75 NET patients, a randomized, blinded consensus read was performed to count tumor lesions on  $^{18}\text{F}$ -AIF-OC and  $^{68}\text{Ga}$ -DOTATATE/NOC PET/CT scans of each patient. The mean differential detection ratio between  $^{18}\text{F}$ -AIF-OC and  $^{68}\text{Ga}$ -DOTATATE/NOC was 15.8% (95% CI: 9.6%–22.0%), meeting the primary non-inferiority objective of the trial and even demonstrating superiority of  $^{18}\text{F}$ -AIF-OC PET.

**IMPLICATIONS FOR PATIENT CARE:**  $^{18}\text{F}$ -AIF-OC is a validated alternative for clinical practice SSTR PET. These results could facilitate widespread implementation of this tracer and increase accessibility for patients.

## REFERENCES

1. Bozkurt MF, Virgolini I, Balogova S, et al. Guideline for PET/CT imaging of neuroendocrine neoplasms with <sup>68</sup>Ga-DOTA-conjugated somatostatin receptor targeting peptides and <sup>18</sup>F-DOPA. *Eur J Nucl Med Mol Imaging*. 2017;44:1588-1601.
2. Hope TA, Bergsland EK, Bozkurt MF, et al. Appropriate use criteria for somatostatin receptor PET imaging in neuroendocrine tumors. *J Nucl Med*. 2018;59:66-74.
3. Pauwels E, Cleeren F, Bormans G, Deroose CM. Somatostatin receptor PET ligands - the next generation for clinical practice. *Am J Nucl Med Mol Imaging*. 2018;8:311-331.
4. Long T, Yang N, Zhou M, et al. Clinical application of <sup>18</sup>F-AIF-NOTA-Octreotide PET/CT in combination with <sup>18</sup>F-FDG PET/CT for imaging neuroendocrine neoplasms. *Clin Nucl Med*. 2019;44:452-458.
5. Pauwels E, Cleeren F, Tshibangu T, et al. [<sup>18</sup>F]AIF-NOTA-octreotide PET imaging: biodistribution, dosimetry and first comparison with [<sup>68</sup>Ga]Ga-DOTATATE in neuroendocrine tumour patients. *Eur J Nucl Med Mol Imaging*. 2020;47:3033-3046.
6. Laverman P, McBride WJ, Sharkey RM, et al. A novel facile method of labeling octreotide with <sup>18</sup>F-fluorine. *J Nucl Med*. 2010;51:454-461.
7. Tshibangu T, Cawthorne C, Serdons K, et al. Automated GMP compliant production of [<sup>18</sup>F]AIF-NOTA-octreotide. *EJNMMI Radiopharm Chem*. 2020;5:4.
8. Hou J, Long T, He Z, et al. Evaluation of <sup>18</sup>F-AIF-NOTA-octreotide for imaging neuroendocrine neoplasms: comparison with <sup>68</sup>Ga-DOTATATE PET/CT. *EJNMMI Res*. 2021;11:55.
9. Kabasakal L, Demirci E, Ocak M, et al. Comparison of <sup>68</sup>Ga-DOTATATE and <sup>68</sup>Ga-DOTANOC PET/CT imaging in the same patient group with neuroendocrine tumours. *Eur J Nucl Med Mol Imaging*. 2012;39:1271-1277.

10. Reubi JC, Schar JC, Waser B, et al. Affinity profiles for human somatostatin receptor subtypes SST1-SST5 of somatostatin radiotracers selected for scintigraphic and radiotherapeutic use. *Eur J Nucl Med.* 2000;27:273-282.
11. Wild D, Macke HR, Waser B, et al. <sup>68</sup>Ga-DOTANOC: a first compound for PET imaging with high affinity for somatostatin receptor subtypes 2 and 5. *Eur J Nucl Med Mol Imaging.* 2005;32:724.
12. Poeppel TD, Binse I, Petersenn S, et al. <sup>68</sup>Ga-DOTATOC versus <sup>68</sup>Ga-DOTATATE PET/CT in functional imaging of neuroendocrine tumors. *J Nucl Med.* 2011;52:1864-1870.
13. Galne A, Almquist H, Almquist M, et al. A prospective observational study to evaluate the effects of long-acting somatostatin analogs on <sup>68</sup>Ga-DOTATATE uptake in patients with neuroendocrine tumors. *J Nucl Med.* 2019;60:1717-1723.

**TABLE 1:** Patient and clinical characteristics (n=75)

<b>Characteristic</b>	<b>Number (%) of patients or Median (range)</b>
Age (y)	65 (37–84)
Sex	
Male	46 (61.3%)
Female	29 (38.7%)
Primary tumor	
Intestine	45 (60.0%)
Pancreas	18 (24.0%)
Lung	7 (9.3%)
CUP	4 (5.3%)
Paraganglioma	1 (1.3%)
Tumor grade	
G1	35 (46.7%)
G1/G2 (i.e. Ki-67<5%)	2 (2.7%)
G2	34 (45.3%)
G3	2 (2.7%)
NA	2 (2.7%)
Ki-67 (%)	2.5 (0.4–29)
Ongoing therapies	
SSA	44 (58.7%)
SSA and everolimus	10 (13.3%)
everolimus	2 (2.7%)
sunitinib	2 (2.7%)
none	17 (22.7%)
Interval between <sup>18</sup> F-AIF-OC and <sup>68</sup> Ga-DOTA-TATE/NOC scan (d)	7 (-30–32)

Ki-67: Ki-67 proliferation index; SSA: somatostatin analog

**TABLE 2:** Comparison between the mean detection ratio with  $^{68}\text{Ga}$ -DOTATATE/NOC ( $\text{DR}_{\text{Ga}}$ ) and  $^{18}\text{F}$ -AIF-OC ( $\text{DR}_{\text{F}}$ ) and mean differential detection ratio (DDR) with 95% confidence interval (95% CI) for the most relevant organs

<b>Organ</b>	<b>mean <math>\text{DR}_{\text{Ga}}</math> (%)</b>	<b>mean <math>\text{DR}_{\text{F}}</math> (%)</b>	<b><i>P</i></b>	<b>mean DDR (%)</b>	<b>95% CI (%)</b>
Liver	60.3	93.3	$<10^{-5}$	33.1	21.7–44.4
Bone	79.8	77.0	0.78	-2.8	-17.8–12.2
Lymph nodes	74.1	96.0	$<10^{-5}$	21.9	14.0–29.8
Lung	73.6	98.1	0.027	24.6	3.3–45.8
Peritoneum	55.5	89.3	0.008	33.8	11.7–55.9
Pancreas	84.6	100.0	0.10	15.4	-3.7–34.4
All (*)	75.3	91.1	$<10^{-5}$	15.8	9.6–22.0

(\*) Lesions in head region not included

**TABLE 3:** Comparison between the mean detection ratio with  $^{68}\text{Ga}$ -DOTATATE and/or -NOC ( $\text{DR}_{\text{Ga}}$ ) and  $^{18}\text{F}$ -AIF-OC ( $\text{DR}_{\text{F}}$ ) and mean differential detection ratio (DDR) with 95% confidence interval (95% CI) for different subgroups of patients according to routine  $^{68}\text{Ga}$ -DOTA-SSA tracer, tumor grade and primary

<b>Subgroup</b>	<b>n</b>	<b>mean <math>\text{DR}_{\text{Ga}}</math> (%)</b>	<b>mean <math>\text{DR}_{\text{F}}</math> (%)</b>	<b><i>P</i></b>	<b>mean DDR (%)</b>	<b>95% CI (%)</b>
$^{68}\text{Ga}$ -DOTATATE	56	77.5	89.4	0.002	11.8	4.3–19.3
$^{68}\text{Ga}$ -DOTANOC	19	68.9	96.4	$<10^{-3}$	27.5	17.8–37.1
G1	35	75.0	89.9	0.003	14.9	6.0–23.8
G2	34	75.5	92.1	0.002	16.6	6.3–27.0
G3	2	62.0	97.4	NA	35.4	NA
Intestine	45	72.6	90.4	$<10^{-3}$	17.8	9.2–26.4
Pancreas	18	84.2	92.7	0.087	8.4	-1.2–18.0

n: number of patients

**TABLE 4:** Mean  $SUV_{max}$  and tumor-to-background ratio (TBR) with  $^{68}\text{Ga}$ -DOTATATE/NOG ( $SUV_{max\_Ga}$ ;  $TBR_{Ga}$ ) and with  $^{18}\text{F}$ -AIF-OC ( $SUV_{max\_F}$ ;  $TBR_F$ ) at patient level for all concordant, quantifiable lesions (n = 3034) and different subsets of lesions

<b>Organ</b>	<b>mean <math>SUV_{max\_Ga}</math></b>	<b>mean <math>SUV_{max\_F}</math></b>	<b><i>P</i></b>	<b>mean <math>TBR_{Ga}</math></b>	<b>mean <math>TBR_F</math></b>	<b><i>P</i></b>
Liver	22.4±11.4	21.5±12.4	0.76	4.8±3.8	6.7±5.2	<10 <sup>-4</sup>
Bone	11.4±8.3	8.6±6.3	0.001	10.1±7.3	13.8±9.9	<10 <sup>-3</sup>
Lymph nodes	20.9±14.3	19.9±16.9	0.19	36.5±24.2	49.9±40.8	0.001
Lung	24.8±29.5	16.9±17.0	0.088	44.0±61.2	42.7±50.4	0.95
Peritoneum	16.3±11.9	14.9±9.9	0.87	29.2±24.4	33.7±25.6	0.091
Pancreas	51.1±38.6	51.9±45.6	0.94	90.3±65.4	141.1±113.8	0.006
Max. 20 per patient	27.7±16.9	24.7±16.3	0.036	29.2±33.1	37.6±40.0	0.001
Max. 5 per organ	28.9±17.9	25.3±16.2	0.032	33.0±33.1	42.3±40.0	0.002
All	22.4±15.6	20.0±14.5	0.067	25.1±32.7	31.7±36.5	0.001

**TABLE 5:** Mean  $SUV_{max}$  and tumor-to-background ratio (TBR) with  $^{68}Ga$ -DOTATATE/NOC ( $SUV_{max\_Ga}$ ;  $TBR_{Ga}$ ) and with  $^{18}F$ -AIF-OC ( $SUV_{max\_F}$ ;  $TBR_F$ ) at patient level for different subgroups of patients according to routine  $^{68}Ga$ -DOTA-SSA tracer, tumor grade and primary

<b>Subgroup</b>	<b>mean <math>SUV_{max\_Ga}</math></b>	<b>mean <math>SUV_{max\_F}</math></b>	<b><i>P</i></b>	<b>mean <math>TBR_{Ga}</math></b>	<b>mean <math>TBR_F</math></b>	<b><i>P</i></b>
$^{68}Ga$ -DOTATATE	23.3±16.9	19.0±14.8	0.002	26.6±36.4	31.8±38.9	0.12
$^{68}Ga$ -DOTANOC	19.6±11.2	23.1±13.7	<10 <sup>-3</sup>	20.7±17.7	31.2±29.2	<10 <sup>-3</sup>
G1	22.9±16.8	17.9±11.5	0.008	26.7±41.4	27.9±36.1	0.20
G2	22.1±14.5	22.4±17.7	0.90	23.3±22.5	35.8±39.2	0.003
G3	15.2±4.2	19.0±0.6	NA	10.3±9.5	15.3±8.7	NA
Intestine	17.8±6.0	16.3±9.4	0.18	17.8±13.0	22.6±20.2	0.008
Pancreas	28.0±16.7	26.9±19.9	0.40	26.3±26.6	40.7±43.9	0.043

**FIGURE 1:** Forest plot summarizing the mean differential detection ratio (DDR) and 95% confidence interval (95% CI), overall and for different subgroups of lesions and patients. The dashed vertical line represents the pre-specified boundary (-15%) for non-inferiority for the lower margin of the 95% CI

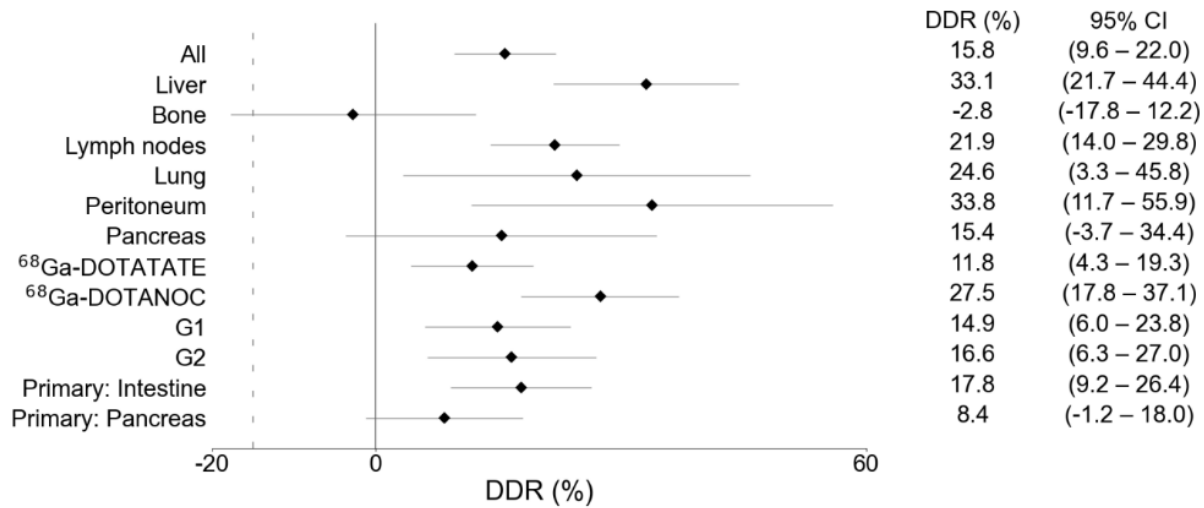


**FIGURE 2:** (A)  $^{68}\text{Ga}$ -DOTATATE and (B)  $^{18}\text{F}$ -AIF-OC images (from top to bottom: maximum-intensity projection PET, transversal PET and fused PET/CT images, respectively) of a 64-year old male patient with pancreatic neuroendocrine tumor and liver, lymph node and peritoneal metastases. Multiple lesions in all three sites were missed by  $^{68}\text{Ga}$ -DOTATATE. Arrows indicate missed liver lesions. Lookup tables apply to PET images (SUV)

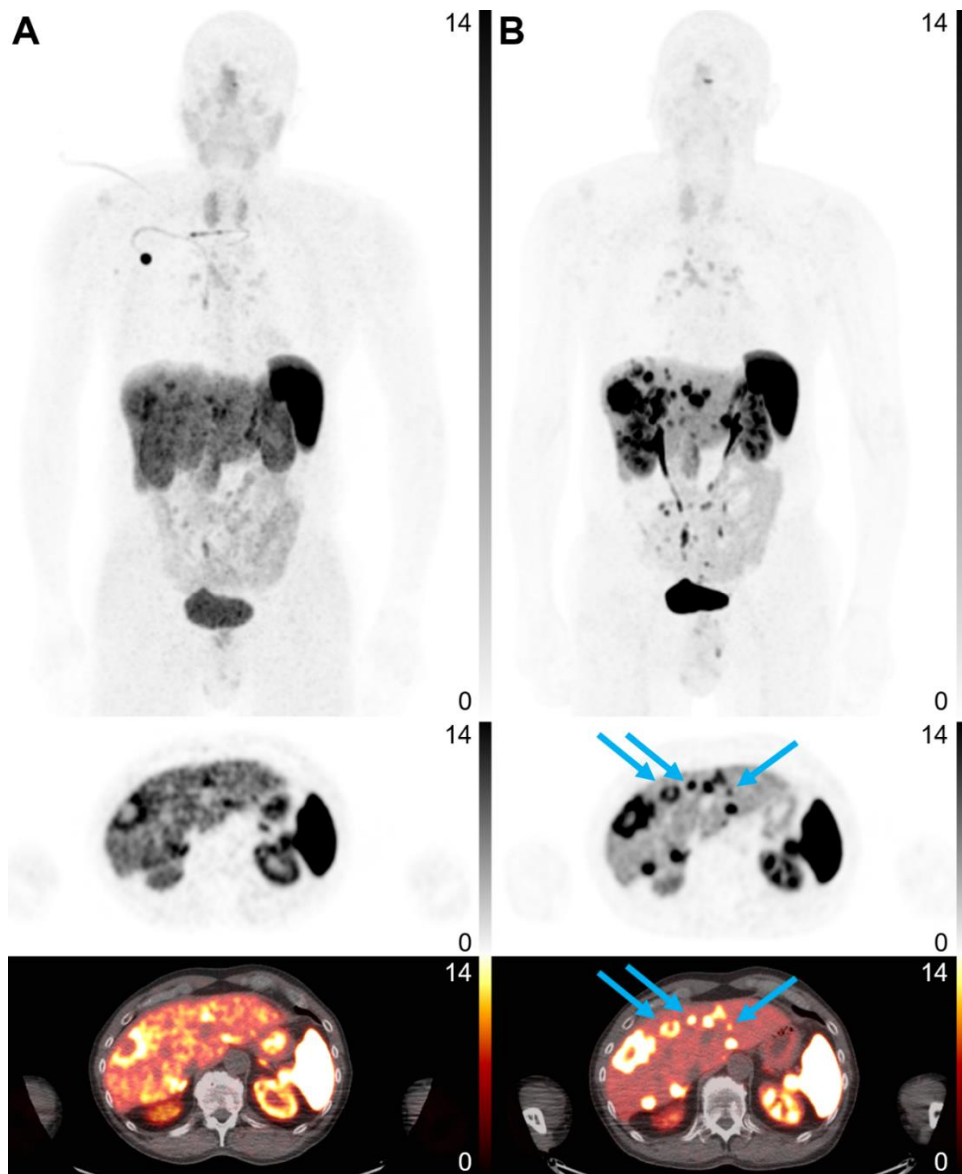


**FIGURE 3:** (A)  $^{68}\text{Ga}$ -DOTATATE and (B)  $^{18}\text{F}$ -AIF-OC images (from top to bottom: maximum-intensity projection PET, transversal PET and fused PET/CT images, respectively) of a 74-year old female patient with an intestinal neuroendocrine tumor and bone, liver, lymph node and peritoneal metastases. Multiple lesions in all three sites were missed by  $^{18}\text{F}$ -AIF-OC. Blue and green arrows indicate missed bone and lymph node lesions, respectively. Lookup tables apply to PET images (SUV)

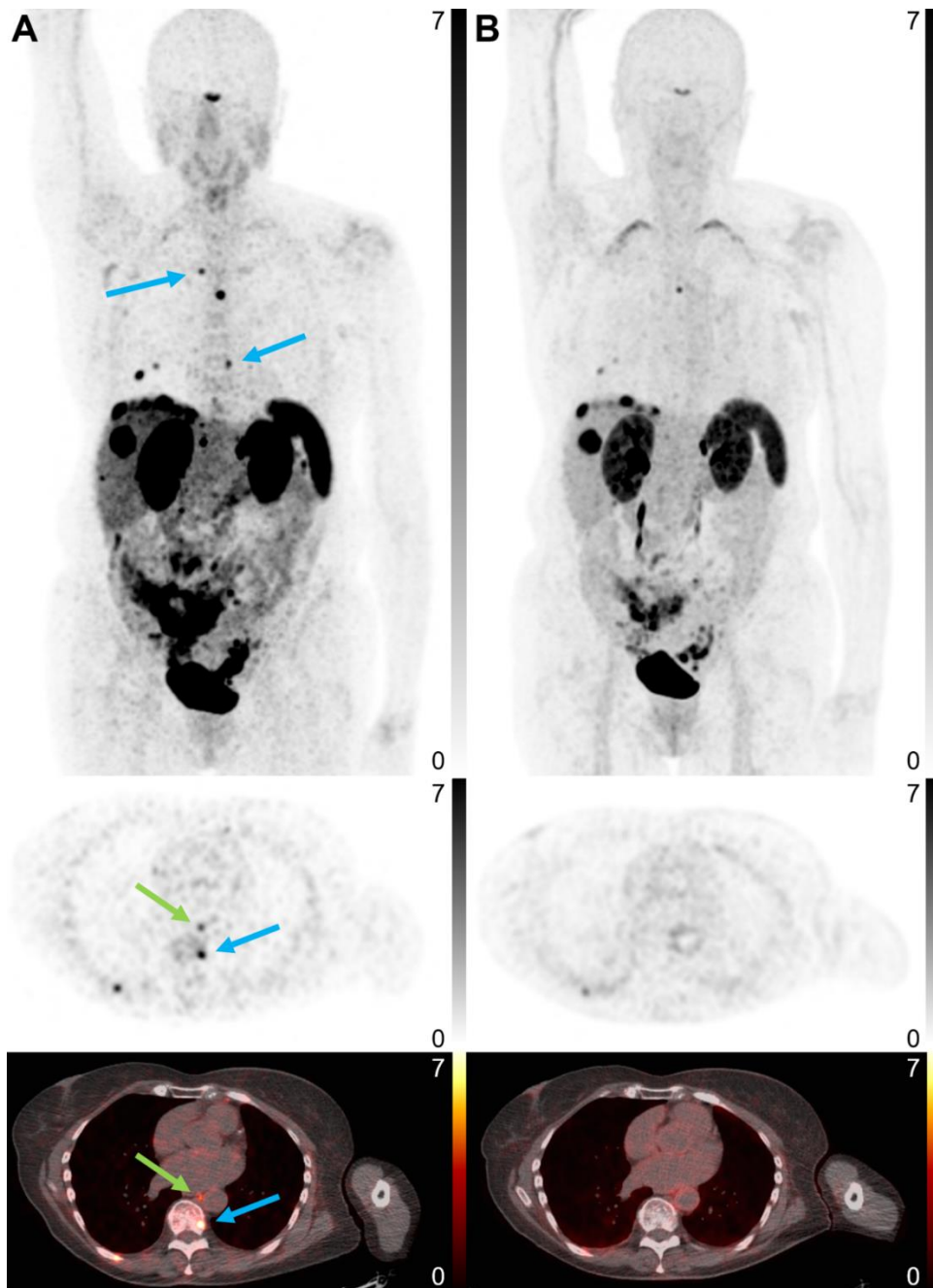
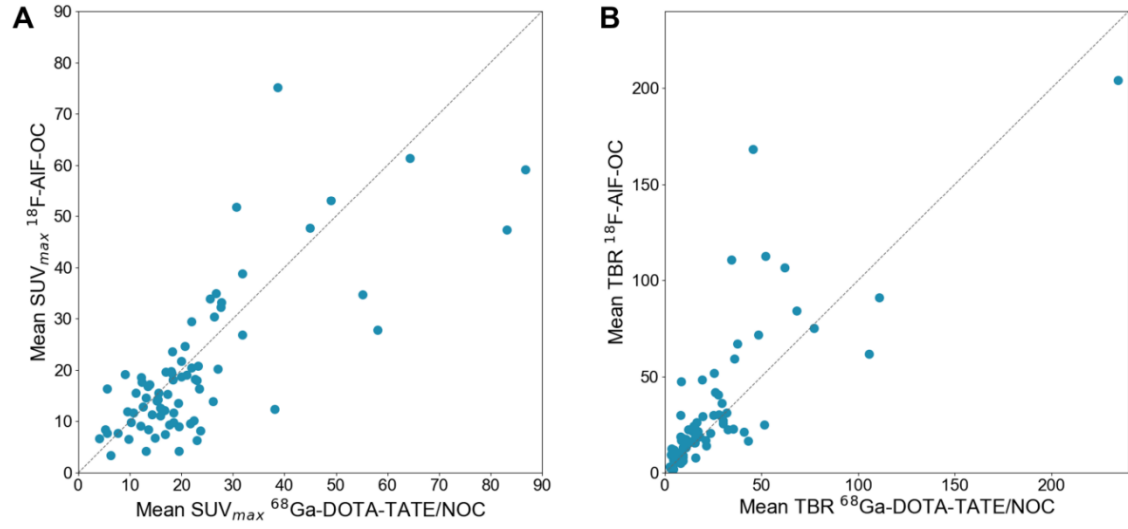
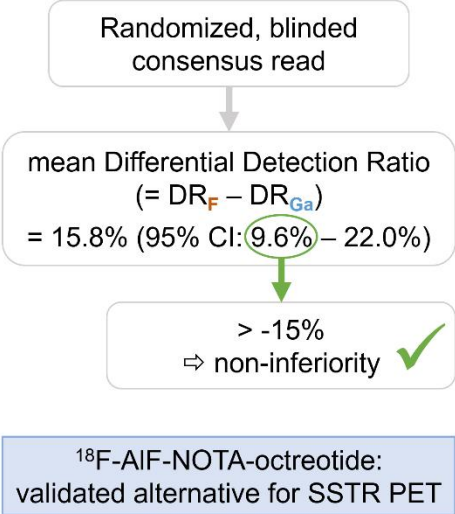
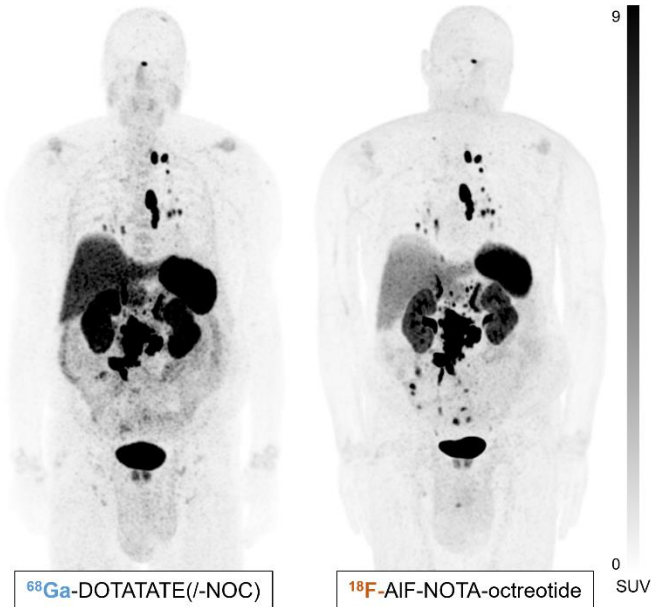


**FIGURE 4:** Mean  $SUV_{max}$  and tumor-to-background ratio (TBR) at patient level with  $^{18}F$ -AIF-OC as a function of mean  $SUV_{max}$  and TBR with  $^{68}Ga$ -DOTATATE/NOC. The gray line represents the unity line



# GRAPHICAL ABSTRACT



# SUPPLEMENTAL INFORMATION

## MATERIALS AND METHODS (*full version*)

### Study Population

In the main part (part A) of this prospective multicenter trial 75 NET patients, aged 18 years or older, were included. The main inclusion criteria were: (1) histologically and/or cytologically confirmed NET of all grades of gastroenteropancreatic, pulmonary, neural crest or unknown primary origin, (2) routine clinical  $^{68}\text{Ga}$ -DOTA-SSA PET/computed tomography (CT) scheduled within three months prior or after the study scan, (3) at least one known tumor lesion below the level of the submandibular and parotid glands, with either a minimum size of 1 cm in at least one dimension on morphological imaging (CT, magnetic resonance imaging (MRI) or ultrasound), or a maximal standardized uptake value ( $\text{SUV}_{\text{max}}$ ) of at least 10 on  $^{68}\text{Ga}$ -DOTA-SSA PET. The main exclusion criterion was previous or ongoing recurrent or chronic disease at high risk to interfere with the performance or evaluation of the trial. The PET/MR part (part B) of the trial in 10 NET patients will be presented elsewhere.

The study was performed at University Hospitals Leuven in collaboration with University Hospital Antwerp and University Hospital Ghent after approval by the Ethics Committee of all three institutes, and all subjects signed a written informed consent (ClinicalTrials.gov identifier NCT04552847).

### Radiosynthesis

$^{18}\text{F}$ -AIF-OC was synthesized in an AllInOne<sup>®</sup> synthesis module (Trasis, Ans, Belgium) according to the procedure described in (7). Validated analytical procedures were applied for quality control (7). The mean radiochemical purity of  $^{18}\text{F}$ -AIF-OC was  $95.1\% \pm 1.5\%$  ( $n = 19$ ). The apparent molar activity at time of injection was  $45.2 \pm 21.5$  GBq/ $\mu\text{mol}$ .

$^{68}\text{Ga}$ -DOTATATE and  $^{68}\text{Ga}$ -DOTANOC were synthesized according to the center's standard operating procedures, using 30  $\mu\text{g}$  of good manufacturing practice-produced DOTATATE (ABX advanced biochemical compounds, Radeberg, Germany) and 50  $\mu\text{g}$  of good manufacturing practice-produced DOTANOC (ABX advanced biochemical compounds) per production, respectively.

### **PET/CT Acquisition**

We previously identified 2 hours post-injection (p.i.) to be the optimal time point for imaging (5). Patients underwent a whole-body PET (from mid-thigh to vertex) 2 hours after intravenous (IV) injection of 4 MBq/kg  $^{18}\text{F}$ -AIF-OC, preceded by a low-dose CT for attenuation correction and anatomical information. Scans were acquired on either a GE Discovery MI 4-ring PET/CT system (GE, Milwaukee, WI, USA) (3 minutes PET acquisition per bed position) or a Siemens Biograph 40 Truepoint TrueV PET/CT system (Siemens Medical, Erlangen, Germany) (4 minutes PET acquisition per bed position). Emission data of the GE system was iteratively reconstructed with the VPFXS algorithm, which makes use of Time-of-Flight information and includes detector response modelling (2 iterations, 34 subsets). Data from the Siemens system was iteratively reconstructed by means of a manufacturer-provided 3D OSEM algorithm with detector response modelling (3 iterations, 21 subsets).

Depending on the center where the routine clinical  $^{68}\text{Ga}$ -DOTA-SSA PET was acquired, either  $^{68}\text{Ga}$ -DOTATATE (n = 56; UZ Leuven) or  $^{68}\text{Ga}$ -DOTANOC (n = 19; UZ Antwerp) was used. The routine PET was performed according to the EANM guidelines (1), with  $^{68}\text{Ga}$ -DOTATATE imaging at 45–60 minutes and  $^{68}\text{Ga}$ -DOTANOC at 60–90 minutes after injection. The mean administered activity was  $139 \pm 27$  MBq  $^{68}\text{Ga}$ -DOTATATE and  $114 \pm 20$  MBq  $^{68}\text{Ga}$ -DOTANOC. PET scans were preceded by a low-dose CT for attenuation correction and anatomical information. The  $^{68}\text{Ga}$ -DOTATATE PET scans for patients in UZ Leuven were matched on the same PET/CT systems as the  $^{18}\text{F}$ -AIF-OC study scan (same reconstruction parameters, same acquisition time for the

Siemens system, 2.5 minutes acquisition per bed position on the GE system).  $^{68}\text{Ga}$ -DOTANOC PET scans for patients in UZ Antwerp were acquired on a GE Discovery MI 4-ring or MI 3-ring PET/CT system (2.5 minutes acquisition per bed position). PET data were reconstructed using the VPFXS algorithm (2 iterations, 17 subsets). The  $^{18}\text{F}$ -AIF-OC study scans for these patients were performed on the GE Discovery MI 4-ring PET/CT system only. All PET/CT systems used in this trial were calibrated using a uniform cylindrical phantom with gallium-68 and dose calibrator settings were adjusted so that the PET systems produce images within 10% of the true SUV. The same was done for fluorine-18 on the UZ Leuven PET/CT systems. To further ensure quantitative comparison between routine and study scans, post-reconstruction filtering of PET images was done using the MIM software package, version 7.1.5 (MIM Software Inc., Cleveland, Ohio, USA) with an isotropic Gaussian smoothing kernel of 5 mm full-width half-maximum for GE system data and 5.5 mm full-width half-maximum for Siemens system data, such that resolution properties were closely matched (based on phantom experiments, data not shown).

For both the routine and study scan, patients were asked to avoid long-acting SSA treatment, except in case of uncontrolled hormonal symptoms, for four to six weeks prior to the scan.

### **Image Analyses**

All image analyses were done using MIM v7.1.5. Tumor lesions were counted in consensus by two experienced readers, blinded for patient data and the radiopharmaceutical that was used. Routine and study scans were randomized per group of 20 patients (40 scans per group) and information regarding patient and radiopharmaceutical was removed from the DICOM headers. Furthermore, since normal salivary gland uptake is markedly higher with  $^{68}\text{Ga}$ -DOTATATE compared with  $^{18}\text{F}$ -AIF-OC (5,8), all PET datasets were trimmed by an independent operator to remove the head region. A positive lesion was defined as a volume of increased tracer uptake compared to background, deemed to be caused by the presence of NET cells, and that is unlikely to be attributed to physiological or benign etiology (e.g. inflammation, blood pool retention,

excretion, etc.). After the randomized, blinded consensus read of each group of 40 scans, the matched pairs of routine and study scans were provided to the readers, without revealing patient and radiopharmaceutical information, so that a few corrections could be made prior to full unblinding. Most importantly, in case multiple distinguishable lesions on one scan were visualized as one confluent lesion on the other scan, the lesion count on the first scan was corrected to one single lesion. Further, lesion count corrections were made for lesions detected on one scan, but not visible on the other due to different trimming of the head region or a different scan field of view (e.g. in the legs). In selected cases, a correction was done for lesions that were discussed during the initial read, but ended up with a different interpretation, e.g. considered as a tumor lesion on one scan and physiological uptake on the other scan, despite a similar aspect on both scans. Finally, operational errors, such as counting the same lesion twice, were corrected.

Following unblinding, the detection ratio (DR) was determined for each scan, i.e. the fraction of lesions detected on that scan, using the union of lesions detected by both tracers ( $^{68}\text{Ga}$ -DOTATATE/NOC and  $^{18}\text{F}$ -AIF-OC) in a patient as the reference. Finally, the differential detection ratio (DDR), which is the difference in DR between  $^{18}\text{F}$ -AIF-OC and  $^{68}\text{Ga}$ -DOTATATE/NOC, was calculated for each patient. The DR at organ level was similarly determined as the number of lesions detected with one tracer divided by all lesions detected by both tracers in a specific organ. For each lesion, the  $\text{SUV}_{\text{max}}$  was measured and the tumor-to-background ratio (TBR) was calculated by dividing the  $\text{SUV}_{\text{max}}$  of that lesion by the  $\text{SUV}_{\text{mean}}$  of relevant background tissue (liver for liver lesions, bone for bone lesions and gluteal muscle for all other lesions). In patients for whom no healthy liver ( $n = 1$ ) or bone tissue ( $n = 2$ ) could be delineated, the mean background value of all other patients was used instead to determine TBRs. Lesions with incorrect attenuation correction due to PET-CT misregistration were excluded from semi-quantitative analysis.

## Outcomes

The primary outcome measure was the DDR. The primary objective, i.e. non-inferiority of  $^{18}\text{F}$ -AIF-OC compared with  $^{68}\text{Ga}$ -DOTATATE/NOC, would be met if the lower margin of the 95% confidence interval (95% CI) for the mean DDR was higher than -15%.

Secondary outcome measures included: lesion uptake in matched pairs of lesions ( $\text{SUV}_{\text{max}}$  and TBR); DR and DDR at organ level; DDR in function of the specific  $^{68}\text{Ga}$ -DOTA-SSA used ( $^{68}\text{Ga}$ -DOTATATE or  $^{68}\text{Ga}$ -DOTANOC) and tumor grade; impact of  $^{18}\text{F}$ -AIF-OC administration on blood pressure and heart rate. A post hoc analysis according to primary tumor site (for  $n > 10$ ) was performed as well.

Lesion uptake was assessed (a) at patient level, (b) for two subsets of hottest lesions, i.e. 20 lesions per patient and maximum 5 lesions per organ, at patient level and (c) at lesion level. Note that for secondary outcome measures, tumor lesions in the head region, identified through non-blinded consensus read, were added in the analyses.

## Statistical Analyses

Statistical analyses were performed using the Python package SciPy (SciPy, RRID:SCR\_008058) and SAS software (version 9.4 of the SAS System for Windows). A power calculation was performed based on a one-sided one-sample t-test. Assuming a standard deviation for the DDR of 17 (based on previous data: (5)), and a mean DDR of zero (i.e. the DR of  $^{18}\text{F}$ -AIF-OC and  $^{68}\text{Ga}$ -DOTATATE/NOC are equal), the power for showing non-inferiority with a sample size of 75 patients was higher than 99%. Assuming a mean DDR of -5% (i.e.  $^{18}\text{F}$ -AIF-OC PET on average 5 percent points worse than  $^{68}\text{Ga}$ -DOTATATE/NOC), the power for showing non-inferiority was higher than 99%. Assuming a mean DDR of -10%, the power for showing non-inferiority was 81%. Number of lesions, DR, background uptake and lesion uptake at patient level (mean  $\text{SUV}_{\text{max}}$  or mean TBR per patient) were compared using a paired sample t-test or Wilcoxon matched-pairs test in case of non-normality, as assessed by a Shapiro-Wilk test. Association between Ki-67 index

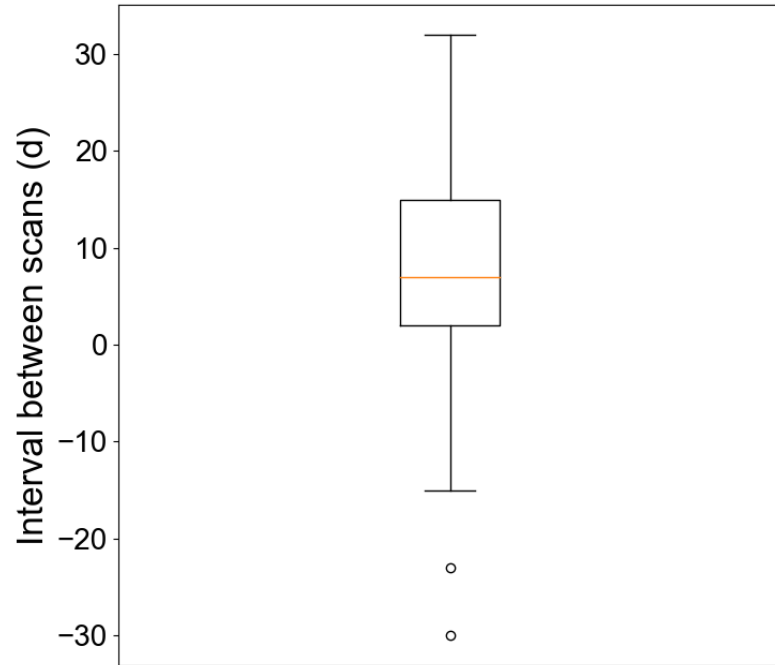
and DDR was assessed with a Spearman correlation coefficient ( $\rho$ ). For tumor uptake at lesion level, linear mixed models were used with the difference in uptake between tracers ( $^{18}\text{F}$ -AIF-OC -  $^{68}\text{Ga}$ -DOTATATE/NOC) as outcome measure. Random intercepts were modelled for patient and organ within patient to account for data clustering. The fixed-effects intercept provided an estimate of the mean difference in lesion uptake between tracers. Normality of the model residuals was checked graphically. Agreement between  $\text{SUV}_{\text{max}}$  at patient level for  $^{18}\text{F}$ -AIF-OC and  $^{68}\text{Ga}$ -DOTATATE/NOC were analyzed with a Bland-Altman plot of mean differences. Two-sided  $P$  values less than 0.05 were considered significant.

## **SAFETY EVALUATION**

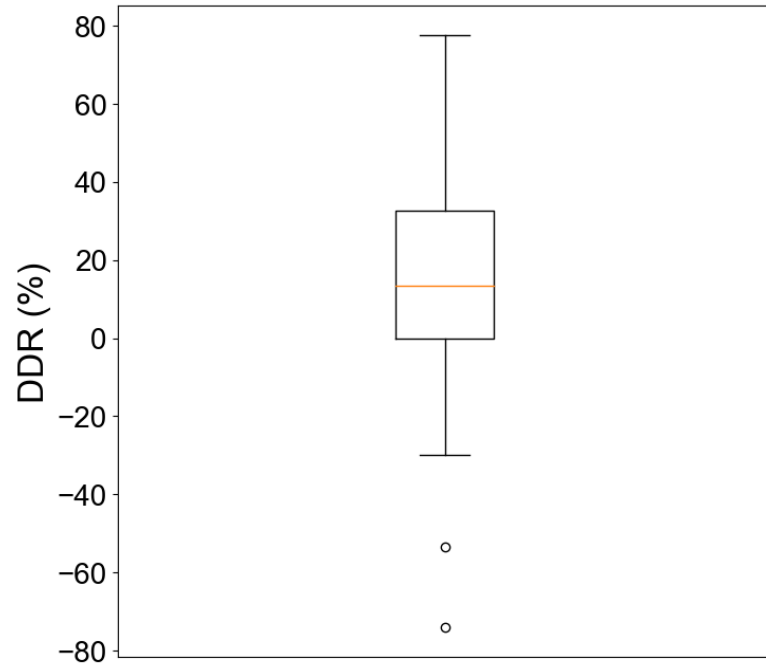
### **Impact of $^{18}\text{F}$ -AIF-OC Administration on Blood Pressure and Heart Rate**

Blood pressure and heart rate were measured prior to  $^{18}\text{F}$ -AIF-OC administration and after the  $^{18}\text{F}$ -AIF-OC PET scan. Adverse events were scored according to the Common Terminology Criteria for Adverse Events (CTCAE) v4.03.

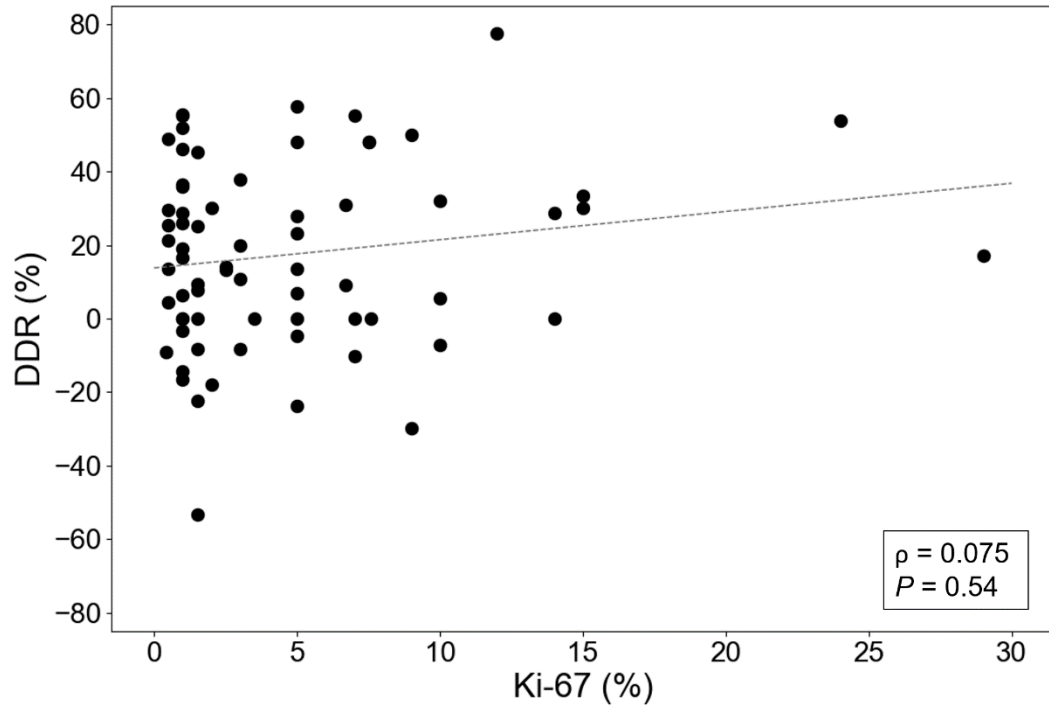
No adverse reactions nor serious adverse events were observed. Twelve grade 1 or 2 adverse events (AEs) and 7 grade 3 AEs (6 from baseline grade 2 and 1 from baseline grade 1) were observed due to pre-existing arterial hypertension. All AEs were asymptomatic and required no therapeutic intervention. On the other hand, 13 patients showed an improvement in blood pressure (3 from baseline grade 3 to grade 2 or 0 and 10 from grade 2 to grade 1). The observed changes in blood pressure can therefore most likely be considered as normal fluctuations in blood pressure in patients with pre-existing arterial hypertension.



**Supplemental Figure 1:** Box-and-whisker plot of the interval between the  $^{18}\text{F}$ -AIF-OC study scan and routine clinical  $^{68}\text{Ga}$ -DOTATATE/NOC scan

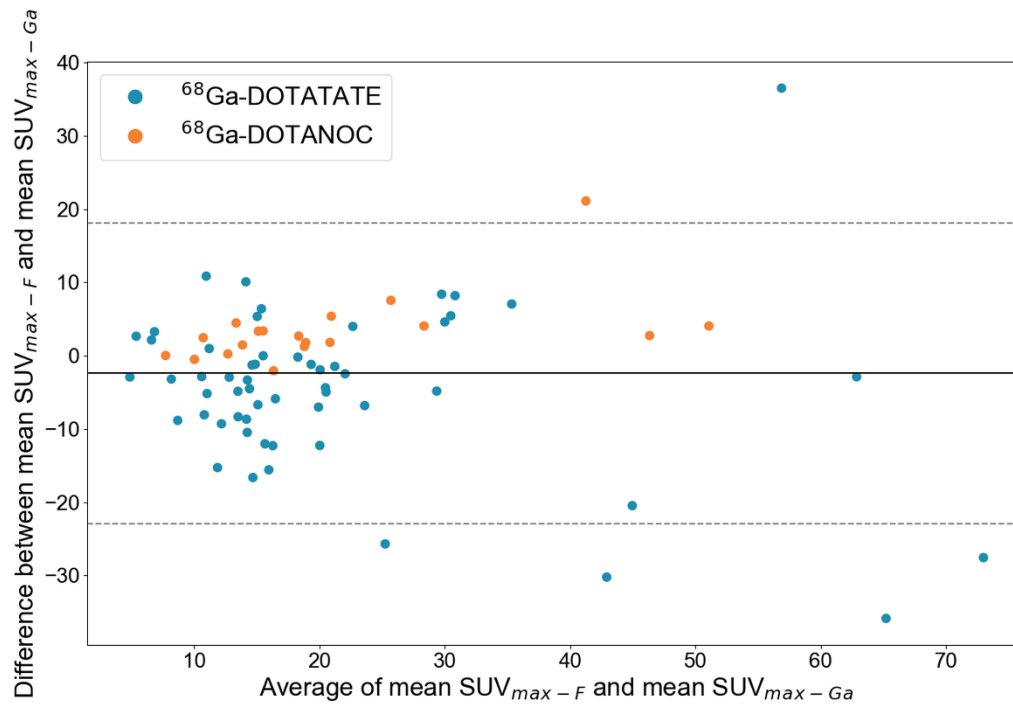


**Supplemental Figure 2:** Box-and-whisker plot of the differential detection rate (DDR)

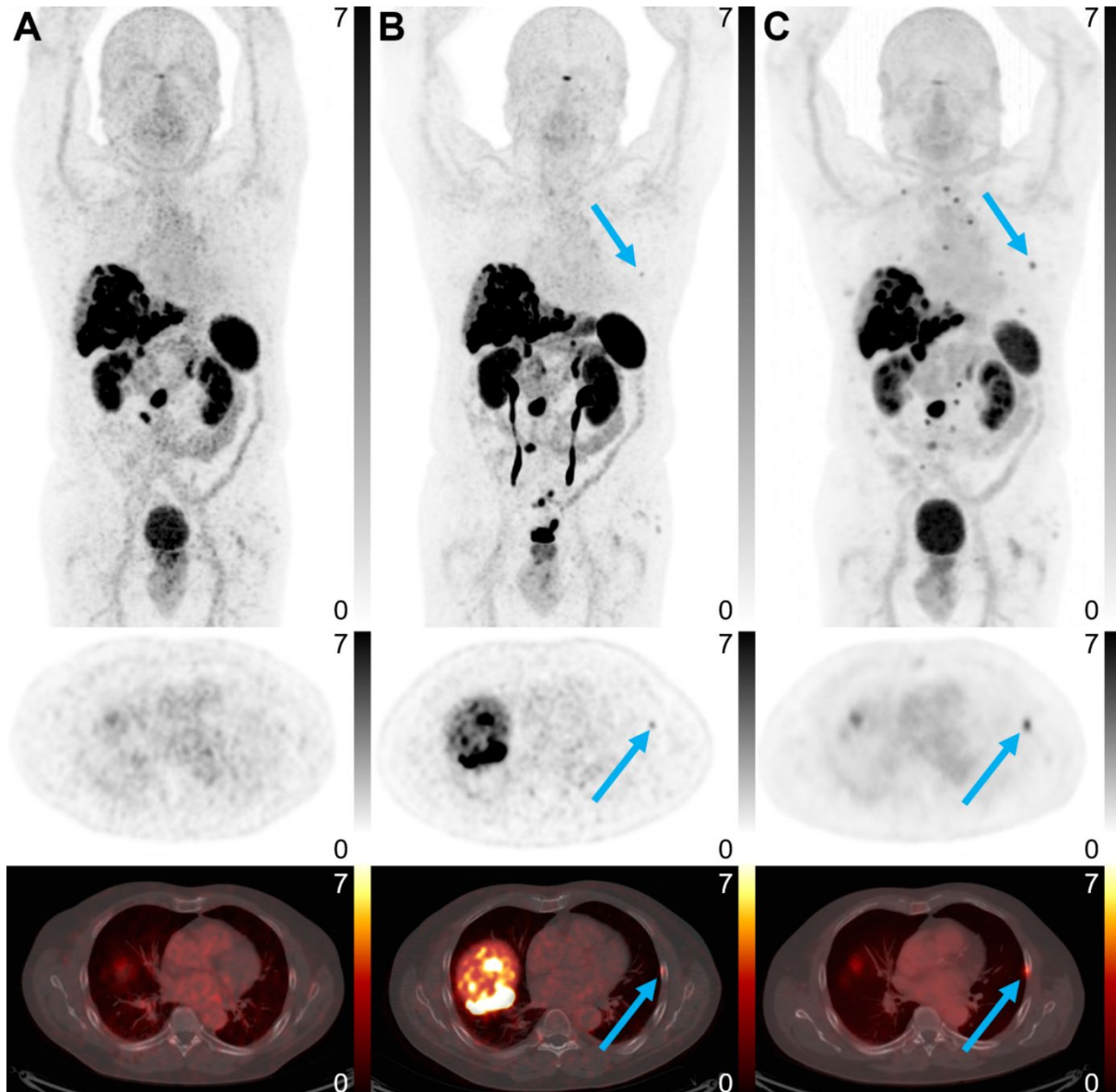


**Supplemental Figure 3:** Differential detection ratio (DDR) as a function of Ki-67 index values.

The gray line represents the regression line.  $\rho$  = Spearman correlation coefficient



**Supplemental Figure 4:** Bland-Altman plot for agreement between mean SUV<sub>max</sub> at patient level with <sup>18</sup>F-AIF-OC (SUV<sub>max\_F</sub>) and mean SUV<sub>max</sub> at patient level with <sup>68</sup>Ga-DOTATATE/NOC (SUV<sub>max\_Ga</sub>). The mean difference was -2.4 (limits of agreement: -22.9–18.1) for all patients, -4.4 (limits of agreement -26.2–17.4) for the <sup>68</sup>Ga-DOTATATE subgroup and 3.4 (limits of agreement: -5.8–12.6) for the <sup>68</sup>Ga-DOTANOC subgroup



**Supplemental Figure 5:** (A)  $^{68}\text{Ga}$ -DOTANOC and (B)  $^{18}\text{F}$ -AIF-OC images (from top to bottom: maximum-intensity projection PET, transversal PET and fused PET/CT images, respectively) of a seventy-year old male patient with an intestinal neuroendocrine tumor with multiple liver metastases and one involved lymph node.  $^{18}\text{F}$ -AIF-OC detected an additional bone lesion (blue arrow) that was confirmed by (C) follow-up  $^{68}\text{Ga}$ -DOTANOC imaging 6 months later. Lookup tables apply to PET images (SUV)

**Supplemental Table 1:** Lesion detection analysis at organ level with a comparison between the number of lesions detected with  $^{68}\text{Ga}$ -DOTATATE/NOC ( $N_{\text{Ga}}$ ) and with  $^{18}\text{F}$ -AIF-OC ( $N_{\text{F}}$ ) and the mean detection ratio with  $^{68}\text{Ga}$ -DOTATATE/NOC ( $\text{DR}_{\text{Ga}}$ ) and  $^{18}\text{F}$ -AIF-OC ( $\text{DR}_{\text{F}}$ )

n: number of patients,  $N_{\text{union}}$ : the total number of lesions detected with both tracers, DDR: differential detection ratio

Organ	n	$N_{\text{union}}$	$N_{\text{Ga}}$	$N_{\text{F}}$	$P$	mean $\text{DR}_{\text{Ga}}$ (%)	mean $\text{DR}_{\text{F}}$ (%)	$P$	mean DDR (%)
Liver	54	1739	1150	1647	$<10^{-6}$	60.3	93.3	$<10^{-5}$	33.1
Bone	50	2012	1712	1727	0.72	79.8	77.0	0.78	-2.8
Lymph nodes	63	602	452	568	$<10^{-5}$	74.1	96.0	$<10^{-5}$	21.9
Lung	18	195	93	193	0.034	73.6	98.1	0.027	24.6
Peritoneum	28	275	158	259	0.002	55.5	89.3	0.008	33.8
Pancreas	13	16	13	16	0.083	84.6	100.0	0.10	15.4
Pleura	2	5	3	3	NA	50.0	66.7	NA	16.7
Small intestine	11	15	12	14	NA	78.8	90.9	NA	12.1
Rectum	2	2	2	2	NA	100.0	100.0	NA	0.0
Soft tissue	3	5	3	5	NA	62.5	100.0	NA	37.5
Muscle	8	26	19	22	NA	77.6	85.3	NA	7.7
Heart	5	17	17	17	NA	100.0	100.0	NA	0.0
Salivary glands	1	2	0	2	NA	0.0	100.0	NA	100.0
Breast	2	2	2	2	NA	100.0	100.0	NA	0.0
Paraganglia	1	8	8	8	NA	100.0	100.0	NA	0.0
Thyroid	1	1	0	1	NA	0.0	100.0	NA	100.0
Stomach	1	1	1	1	NA	100.0	100.0	NA	0.0
All <sup>(*)</sup>	75	4923	3645	4487	$<10^{-4}$	75.7	91.4	$<10^{-5}$	15.7

<sup>(\*)</sup> Lesions in head region included

**Supplemental Table 2:** Lesion detection analysis for the subgroup of patients scanned with  $^{68}\text{Ga}$ -DOTATATE with a comparison between the number of lesions detected with  $^{68}\text{Ga}$ -DOTATATE ( $N_{\text{Ga}}$ ) and with  $^{18}\text{F}$ -AIF-OC ( $N_{\text{F}}$ ) and the mean detection ratio with  $^{68}\text{Ga}$ -DOTATATE ( $\text{DR}_{\text{Ga}}$ ) and  $^{18}\text{F}$ -AIF-OC ( $\text{DR}_{\text{F}}$ )

n: number of patients,  $N_{\text{union}}$ : the total number of lesions detected with both tracers, DDR: differential detection ratio

Organ	n	$N_{\text{union}}$	$N_{\text{Ga}}$	$N_{\text{F}}$	$P$	mean $\text{DR}_{\text{Ga}}$ (%)	mean $\text{DR}_{\text{F}}$ (%)	$P$	mean DDR (%)
Liver	38	1084	728	999	$<10^{-3}$	57.7	92.3	$<10^{-4}$	34.5
Bone	39	1828	1633	1544	0.30	90.5	71.4	0.020	-19.2
Lymph nodes	47	469	356	436	$<10^{-3}$	75.0	94.7	$<10^{-3}$	19.7
Lung	14	189	90	187	0.058	73.1	97.6	0.046	24.4
Peritoneum	24	218	127	203	0.006	53.1	87.6	0.019	34.5
Pancreas	10	12	10	12	0.16	85.0	100.0	0.18	15.0
Pleura	1	3	3	1	NA	100.0	33.3	NA	-66.7
Small intestine	6	9	7	9	NA	78.8	100.0	NA	22.2
Rectum	2	2	2	2	NA	100.0	100.0	NA	0.0
Soft tissue	3	4	2	4	NA	50.0	100.0	NA	50.0
Muscle	6	24	17	20	NA	70.1	80.4	NA	10.3
Heart	3	14	14	14	NA	100.0	100.0	NA	0.0
Salivary glands	1	2	0	2	NA	0.0	100.0	NA	100.0
Breast	2	2	2	2	NA	100.0	100.0	NA	0.0
Paraganglia	1	8	8	8	NA	100.0	100.0	NA	0.0
Thyroid	1	1	0	1	NA	0.0	100.0	NA	100.0
Stomach	1	1	1	1	NA	100.0	100.0	NA	0.0
All <sup>(*)</sup>	56	3870	3000	3445	0.003	77.9	89.8	0.002	11.8

<sup>(\*)</sup> Lesions in head region included

**Supplemental Table 3:** Lesion detection analysis for the subgroup of patients scanned with  $^{68}\text{Ga}$ -DOTANOC with a comparison between the number of lesions detected with  $^{68}\text{Ga}$ -DOTANOC ( $N_{\text{Ga}}$ ) and with  $^{18}\text{F}$ -AIF-OC ( $N_{\text{F}}$ ) and the mean detection ratio with  $^{68}\text{Ga}$ -DOTANOC ( $\text{DR}_{\text{Ga}}$ ) and  $^{18}\text{F}$ -AIF-OC ( $\text{DR}_{\text{F}}$ )

n: number of patients,  $N_{\text{union}}$ : the total number of lesions detected with both tracers, DDR: differential detection ratio

Organ	n	$N_{\text{union}}$	$N_{\text{Ga}}$	$N_{\text{F}}$	$P$	mean $\text{DR}_{\text{Ga}}$ (%)	mean $\text{DR}_{\text{F}}$ (%)	$P$	mean DDR (%)
Liver	16	655	422	648	0.002	66.4	95.9	0.002	29.5
Bone	11	184	79	183	0.007	41.7	97.0	0.008	55.2
Lymph nodes	16	133	96	132	0.005	71.4	99.8	0.005	28.4
Lung	4	6	3	6	0.32	75.0	100.0	0.32	25.0
Peritoneum	4	57	31	56	0.10	70.0	99.5	0.11	29.5
Pancreas	3	4	3	4	0.32	83.3	100.0	0.32	15.0
Pleura	1	2	0	2	NA	0.0	100.0	NA	100.0
Small intestine	5	6	5	5	NA	80.0	80.0	NA	0.0
Soft tissue	1	1	1	1	NA	100.0	100.0	NA	0.0
Muscle	2	2	2	2	NA	100.0	100.0	NA	0.0
Heart	2	3	3	3	NA	100.0	100.0	NA	0.0
All <sup>(*)</sup>	19	1053	645	1042	$<10^{-3}$	69.1	96.4	$<10^{-3}$	27.2

<sup>(\*)</sup> Lesions in head region included

**Supplemental Table 4:** Comparison of background uptake with  $^{68}\text{Ga}$ -DOTATATE and/or -NOC ( $\text{SUV}_{\text{mean\_Ga}}$ ) and with  $^{18}\text{F}$ -AIF-OC ( $\text{SUV}_{\text{mean\_F}}$ ) for all patients and subgroups of patients according to routine  $^{68}\text{Ga}$ -DOTA-SSA tracer, tumor grade<sup>(\*)</sup> and primary

Subgroup	Background tissue	$\text{SUV}_{\text{mean\_Ga}}$	$\text{SUV}_{\text{mean\_F}}$	<i>P</i>
All patients	Liver	6.3 ± 2.5	4.2 ± 1.7	<10 <sup>-7</sup>
	Bone	1.2 ± 0.5	0.7 ± 0.2	<10 <sup>-7</sup>
	Muscle	0.6 ± 0.2	0.4 ± 0.1	<10 <sup>-7</sup>
$^{68}\text{Ga}$ -DOTATATE	Liver	6.9 ± 2.5	4.2 ± 1.8	<10 <sup>-7</sup>
	Bone	1.4 ± 0.5	0.7 ± 0.2	<10 <sup>-7</sup>
	Muscle	0.6 ± 0.2	0.5 ± 0.1	<10 <sup>-7</sup>
$^{68}\text{Ga}$ -DOTANOC	Liver	4.5 ± 1.9	4.1 ± 1.4	0.10
	Bone	0.8 ± 0.2	0.6 ± 0.1	<10 <sup>-3</sup>
	Muscle	0.5 ± 0.1	0.4 ± 0.1	<10 <sup>-3</sup>
G1	Liver	6.5 ± 2.3	4.2 ± 1.6	<10 <sup>-7</sup>
	Bone	1.3 ± 0.5	0.7 ± 0.2	<10 <sup>-6</sup>
	Muscle	0.6 ± 0.2	0.4 ± 0.1	<10 <sup>-6</sup>
G2	Liver	5.9 ± 2.9	4.0 ± 1.8	<10 <sup>-4</sup>
	Bone	1.1 ± 0.4	0.7 ± 0.2	<10 <sup>-6</sup>
	Muscle	0.6 ± 0.2	0.4 ± 0.1	<10 <sup>-7</sup>
Intestine	Liver	5.7 ± 2.1	3.8 ± 1.5	<10 <sup>-7</sup>
	Bone	1.3 ± 0.5	0.6 ± 0.2	<10 <sup>-7</sup>
	Muscle	0.6 ± 0.1	0.4 ± 0.1	<10 <sup>-7</sup>
Pancreas	Liver	6.5 ± 2.4	4.3 ± 1.7	<10 <sup>-5</sup>
	Bone	1.2 ± 0.4	0.7 ± 0.2	<10 <sup>-4</sup>
	Muscle	0.6 ± 0.2	0.5 ± 0.2	<10 <sup>-5</sup>

<sup>(\*)</sup> The G3 subgroup was omitted as it contains only two patients

**Supplemental Table 5:** Mean  $SUV_{max}$  and tumor-to-background ratio (TBR) with  $^{68}Ga$ -DOTATATE/NOC ( $SUV_{max\_Ga}$ ;  $TBR_{Ga}$ ) and with  $^{18}F$ -AIF-OC ( $SUV_{max\_F}$ ;  $TBR_F$ ) at patient level for all concordant, quantifiable lesions (n = 3034) per organ

Organ	mean $SUV_{max\_Ga}$	mean $SUV_{max\_F}$	mean $TBR_{Ga}$	mean $TBR_F$
Liver	22.4 ± 11.4	21.5 ± 12.4	4.8 ± 3.8	6.7 ± 5.2
Bone	11.4 ± 8.3	8.6 ± 6.3	10.1 ± 7.3	13.8 ± 9.9
Lymph nodes	20.9 ± 14.3	19.9 ± 16.9	36.5 ± 24.2	49.9 ± 40.8
Lung	24.8 ± 29.5	16.9 ± 17.0	44.0 ± 61.2	42.7 ± 50.4
Peritoneum	16.3 ± 11.9	14.9 ± 9.9	29.2 ± 24.4	33.7 ± 25.6
Pancreas	51.1 ± 38.6	51.9 ± 45.6	90.3 ± 65.4	141.1 ± 113.8
Pleura	14.6	5.7	29.8	14.6
Small intestine	20.7 ± 13.1	24.2 ± 17.2	34.4 ± 15.8	52.3 ± 29.3
Rectum	16.8 ± 17.1	21.4 ± 16.1	49.8 ± 61.5	137.1 ± 162.3
Soft tissue	6.9 ± 2.5	7.3 ± 3.0	13.0 ± 4.0	24.1 ± 11.8
Muscle	4.4 ± 3.0	4.2 ± 1.6	8.1 ± 5.6	14.6 ± 9.6
Heart	12.7 ± 10.5	13.3 ± 11.4	23.0 ± 20.1	32.1 ± 26.5
Breast	6.8 ± 5.8	9.5 ± 8.9	11.1 ± 6.4	18.6 ± 12.8
Paraganglia	58.9	35.6	83.0	77.3

**Supplemental Table 6:** Mean  $SUV_{max}$  and tumor-to-background ratio (TBR) with  $^{68}Ga$ -DOTATATE and/or -NOC ( $SUV_{max_{Ga}}$ ;  $TBR_{Ga}$ ) and with  $^{18}F$ -AIF-OC ( $SUV_{max_{F}}$ ;  $TBR_{F}$ ) per organ (at patient level) for subgroups of patients according to routine  $^{68}Ga$ -DOTA-SSA tracer, tumor grade(\*) and primary

Subgroup	Organ	mean $SUV_{max_{Ga}}$	mean $SUV_{max_{F}}$	<i>P</i>	mean $TBR_{Ga}$	mean $TBR_{F}$	<i>P</i>
$^{68}Ga$ -DOTATATE	Liver	23.9 ± 12.0	21.4 ± 13.2	0.10	4.8 ± 4.3	7.1 ± 5.8	<10 <sup>-3</sup>
	Bone	12.3 ± 8.8	8.4 ± 6.6	<10 <sup>-4</sup>	9.8 ± 7.7	13.4 ± 10.7	0.012
	Lymph nodes	21.0 ± 15.1	18.5 ± 17.4	0.011	35.7 ± 25.4	46.9 ± 43.5	0.10
	Lung	28.3 ± 31.6	18.5 ± 18.4	0.071	50.7 ± 66.6	47.6 ± 55.2	0.64
	Peritoneum	16.4 ± 13.1	14.2 ± 10.5	0.78	29.8 ± 26.9	32.0 ± 27.7	0.33
	Pancreas	50.2 ± 40.5	50.9 ± 49.9	0.86	82.0 ± 59.4	137.5 ± 121.1	0.087
$^{68}Ga$ -DOTANOC	Liver	19.3 ± 9.4	21.9 ± 10.8	0.002	4.7 ± 2.2	5.9 ± 3.6	0.015
	Bone	8.0 ± 5.0	9.4 ± 5.2	0.067	11.1 ± 6.3	15.3 ± 6.0	0.002
	Lymph nodes	20.6 ± 12.1	24.6 ± 14.6	0.033	39.2 ± 20.3	59.8 ± 29.2	<10 <sup>-3</sup>
	Lung	10.5 ± 14.3	10.5 ± 9.7	0.99	17.4 ± 22.1	23.1 ± 17.5	0.17
	Peritoneum	15.8 ± 7.3	17.6 ± 8.0	0.029	27.2 ± 13.6	40.2 ± 16.7	0.081
	Pancreas	53.6 ± 40.3	54.8 ± 37.6	0.62	115.4 ± 90.4	152.0 ± 111.2	0.11
G1	Liver	19.7 ± 7.0	17.0 ± 7.3	0.061	3.7 ± 1.7	5.1 ± 3.0	0.008
	Bone	11.5 ± 8.4	7.6 ± 4.2	0.008	9.5 ± 6.0	12.0 ± 6.9	0.098
	Lymph nodes	20.3 ± 11.9	17.5 ± 11.3	0.10	36.2 ± 21.9	41.2 ± 24.3	0.062
G2	Liver	25.4 ± 14.5	25.7 ± 15.4	0.55	6.0 ± 4.9	8.4 ± 6.4	0.002
	Bone	11.3 ± 8.7	9.3 ± 7.3	0.067	10.5 ± 8.4	15.4 ± 11.9	0.021
	Lymph nodes	19.4 ± 13.1	20.9 ± 20.2	0.87	34.1 ± 22.7	56.3 ± 50.4	0.007
Intestine	Liver	19.2 ± 7.0	17.9 ± 8.5	0.34	4.0 ± 1.7	5.9 ± 4.6	0.004
	Bone	10.7 ± 7.5	8.7 ± 6.9	0.016	9.0 ± 5.9	14.3 ± 11.6	<10 <sup>-3</sup>
	Lymph nodes	20.0 ± 12.1	18.2 ± 12.2	0.20	36.8 ± 21.4	45.0 ± 27.7	0.018
Pancreas	Liver	30.9 ± 15.9	29.9 ± 16.8	0.97	6.6 ± 6.3	8.5 ± 6.5	0.006
	Bone	12.6 ± 8.6	9.4 ± 6.7	0.051	12.3 ± 10.8	14.1 ± 7.4	0.44
	Lymph nodes	21.9 ± 14.4	23.3 ± 23.9	0.68	35.8 ± 24.8	62.8 ± 59.3	0.11

(\*) The G3 subgroup was omitted as it contains only two patients